Research Article

Empirical compliance equations for conventional single-axis flexure hinges

Yunsong Du[1] · Tiemin Li[2]

Received: 8 April 2019 / Accepted: 17 October 2019 / Published online: 24 October 2019

Abstract
In consideration of the stress concentration, unified compliance equations for conventional single-axis hinges are presented. The relationship between the stress concentration and the compliance of corner-filleted flexure hinges is first analyzed. Considering the stress concentration, coupled with a wide range of geometrical parameters, empirical compliance equations for conventional flexure hinges, are then obtained by using the exponential model. Subsequently, the proposed equations are unified. To verify the validity and accuracy of these equations, the characteristics of a bridge-type flexure-based mechanism are then analyzed by the proposed equations and finite element analysis, respectively. The results of compliances and displacement amplification ratios obtained by these two methods are in good agreement. It demonstrates that the empirical compliance equations could be obtained by exponential model, and these equations can be unified.

Keywords Flexure hinge · Empirical compliance equations · Exponential model · Compliance · Compliant mechanism

1 Introduction

A flexure hinge, coupled with elastically regions and rigid beams, is a thin member that provides the relative rotation between two adjacent rigid beams [1]. These hinges possess notable benefits such as no hysteresis, no friction losses, no need for lubrication, and ease of fabrication [1–7]. Therefore, flexure hinges have been widely used in various areas, such as automobile and aviation industries, inertial navigation industries, biomedical industries, computers and fiberoptics industries, and so on [8–13]. These hinges are the basic elements of the flexure-based mechanisms, which can be applied to a wide range of applications. For example, accelerometers are key components of inertial navigation systems. In order to guarantee the accuracy of accelerometers, these flexure hinges are used to test accelerometer transverse sensitivity. In biomedical industries, they have been used to be key components of scanners. They are designed based on three piezoelectric actuators and several flexure hinges. In order to obtain high frequency in all three axes, a compact and rigid structure should be adopted.

The compliance of flexure hinges can influence the mechanical design, topology optimization, and dynamic accuracy of flexure-based mechanisms [14]. Thus, many compliance equations for flexure hinges have been obtained to reduce the compliance modeling errors of flexure-based mechanisms, including polynomial approximation method, Castigliano's theorem, and empirical equations obtained from FEA [15, 16]. Paros and Weisbord [17] introduced compliance equations for circular hinges, and these equations were simply and accurate. Smith et al. [18] presented empirical equations for elliptical hinges, and the characteristics were then verified by FEA. The prototype hinges were fabricated by a CNC milling machine. Subsequently, the bending moment was

✉ Yunsong Du, duyunsongwei@163.com | [1]College of Mechanical Engineering and Applied Electronics Technology, Beijing University of Technology, Beijing 100124, China. [2]Department of Mechanical Engineering, Manufacturing Engineering Institute, Tsinghua University, Beijing 100084, China.

applied on the developed hinges, and the compliance of the hinge obtained by experiments was in good agreement with the theoretical arithmetic derived from those equations. Tian [19] introduced dimensionless empirical equations and graph expressions of three kinds of flexure hinges. The relationship between performances and geometrical parameters were then discussed, and empirical equations were obtained by the least square polynomial approximation method. At last, the characteristics of the three hinges were compared which could provide designers with a thorough understanding of these hinges and flexure-based mechanisms. Lobontiu et al. [20] investigated the characteristics of corner-filleted hinges. And compliance equations were obtained by employing the castigliano's first theorem. The relationship between the performance derived from these equations and geometrical parameters was then discussed. It indicated that the proposed equations were accurate and cost-effective. In addition, the theoretical results were compared to experimental values, and the errors were less than 8%. Meng [21] focused on the corner-filleted flexure hinge, and its stiffness/compliance equations were presented. According to the FEA results, three stiffness/compliance equations with a wide range of geometrical parameters were obtained to overcome the influence induced by shearing. The comparisons with FEA indicated that the proposed empirical stiffness/compliance equations could enlarge the range of hinge thickness to hinge length. In addition, it could also improve the accuracy under large deformation. Yong [22] focused on the characteristics of circular hinges, and discussed the difference of the various compliance equations by using FEA. These equations were derived by different methods, and could be used in certain conditions. A proper scheme was then proposed to choose accurate equations according to the comparison. Subsequently, the empirical compliance equations, coupled with a large range of hinge parameters (hinge thickness/hinge radius), were obtained.

However, these proposed methods ignore the influence of the stress concentration caused by changes in cross-section of flexure hinges, and few have got unified equations for conventional single-axis flexure hinges. In this work, the influence of the stress concentration caused by changes in cross-section is taken into account, and the empirical compliance equations can be determined by using FEA. Subsequently, the equations for different hinges determined by this method can be unified. In addition, the characteristics of a bridge-type flexure-based mechanism are discussed, which can verify the method and the corresponding equations.

The remaining sections are organized as follows. In Sect. 2, the compliance matrices of single-axis hinges are introduced. In Sect. 3, the relationship between stress concentration and the compliance of corner-filleted ones is discussed, and then the derivation of the empirical compliance equations is described. In Sect. 4, the compliances of circular and rectangular ones are determined. In Sect. 5, unified empirical compliance equations are derived. In Sect. 6, amplification ratios of a flexure-based mechanism determined by FEA and empirical compliance equations are compared.

2 Single-axis flexure hinges

Single-axis flexure hinges, coupled with a constant width, contain corner-filleted, rectangular, elliptical, and so on. As illustrated in Fig. 1, a typical single-axis flexure hinge is comprised of the flexure hinge with a constant width and two rigid beams. The origin of the coordinate system *xyz* is located at the free end of the left rigid beam. The *x*-axis is in the longitudinal direction of the hinge, while the *y*-axis is in the height direction. Generally, the flexure hinge between the two rigid beams can be applied by a load with six components: two shearing forces, F_y, F_z; two bending moments, M_y, M_z; a force along the *x*-axis, F_x; and a moment around the *x*-axis, M_x. For two-dimensional applications, where all active and resistive loads are planar, only the in-plane components M_z, F_y and F_x have substantive effects on the flexure operation. The other components specified are out-of-plane agents that usually have a lesser magnitude, and therefore impact, on the flexure [1].

The deformation caused by the external load applied at the free end point *a* of the proposed hinge could be written as

$$\delta = CF \tag{1}$$

where δ denotes the total deformation generated at the point *a*, *F* denotes an external load at the end point *a*, and *C* denotes the compliance.

Considering that the load, deformation, and compliance is comprised of in-plane and out-of-plane submatrices, the deformation can be also expressed as

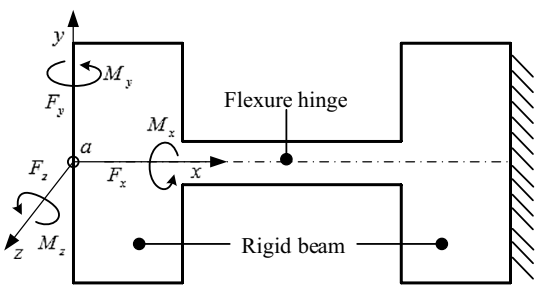

Fig. 1 External loads of the single-axis flexure hinge

$$\begin{bmatrix} \delta^{in} \\ \delta^{out} \end{bmatrix} = \begin{bmatrix} \boldsymbol{C}^{in} & 0 \\ 0 & \boldsymbol{C}^{out} \end{bmatrix} \begin{bmatrix} \boldsymbol{F}^{in} \\ \boldsymbol{F}^{out} \end{bmatrix} \tag{2}$$

where $\boldsymbol{\delta}^{in} = [\boldsymbol{\delta}_x, \boldsymbol{\delta}_y, \alpha_z]^T$ and $\boldsymbol{\delta}^{out} = [\boldsymbol{\delta}_z, \alpha_y]^T$ are the in-plane and out-of-plane deformation at the end point o, $F^{in} = [F_x, \boldsymbol{F}_y, M_z]^T$ and $F^{out} = [\boldsymbol{F}_z, M_y]^T$ are the in-plane and out-of-plane external load, respectively.

The proposed two compliance matrices can be expressed as, respectively

$$\boldsymbol{C}^{in} = \begin{bmatrix} C_{x-F_x} & 0 & 0 \\ 0 & C_{y-F_y} & C_{y-M_z} \\ 0 & C_{\alpha_z-F_y} & C_{\alpha_z-M_z} \end{bmatrix} \tag{3}$$

$$\boldsymbol{C}^{out} = \begin{bmatrix} C_{z-F_z} & C_{z-M_y} \\ C_{\alpha_y-F_z} & C_{\alpha_y-M_y} \end{bmatrix} \tag{4}$$

where $\boldsymbol{C}_{m-n}$ denotes the compliance generated along the direction m caused by the load n.

3 Corner-filleted flexure hinges

Corner-filleted flexure hinges are very conventional. Their geometrical parameters are shown in Fig. 2. R denotes the radius of flexure hinge, t denotes the thickness, L denotes the length, W is the width, D is the depth, and H is the height.

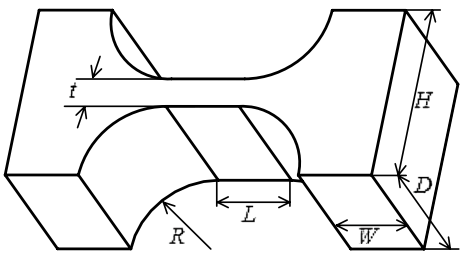

Fig. 2 Geometrical parameters of a corner-filleted flexure hinge

3.1 The influence of the stress concentration

The stress and strain distribution caused by the unit axial load should be first analyzed to investigate and explain the compliance calculation errors. Without loss of generality, $L = 5$ mm, $W = 30$ mm, $R = 5$ mm, $t = 2$ mm, and $D = 10$ mm. FEA model is carried on by the software ANSYS 14.0. As shown in Fig. 3, the left rigid beam is fixed, while the right rigid beam is free, and the load (1 N) is applied on the free end. The stress and strain of the surfaces with same colors are equal, and the surfaces with equal stress and strain are not vertical to the x-axis, and they are also not parallel to each other, which is inconsistent with the basic theoretical stress assumptions. The reason is that the cross-section changes along the flexure hinge, which can affect the stress distribution, so that the basic theoretical stress analysis equations are no longer applied. Such changes in cross-section cause a local increase of stress, referred to as stress concentration. Therefore, the proposed stress concentration can lead to the compliance calculation errors.

To explain the phenomenon clearly, the axial stress distribution obtained by FEA and basic theoretical stress assumptions along the x-axis of a selected flexure hinge, can be compared in Fig. 4. The load (1 N) is applied on the free end, and the FEA stress is used as a benchmark for comparing with the theoretical stress. Compared with the theoretical values, the FEA values are larger at the locations where cross-section changes, which is in accordance with the distribution of the stress concentration.

As shown in Fig. 5, a corner-filleted one, coupled with particular rigid beams, must be selected to further investigate stress concentration. And it is comprised of three main parts: rectangle hinge with a constant width, rigid beams next to flexure hinge, and rigid beams away from flexure hinge. Then, the compliance proportions (ratios of total compliance) and compliance calculation errors of the second and third parts are discussed.

The compliance proportions and compliance calculation errors of the second parts are shown in Fig. 6. The compliance proportions of the three main compliance components increase, including bending compliance

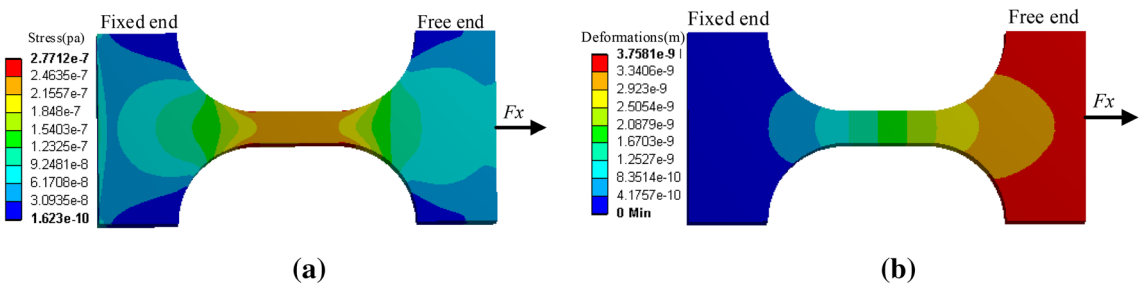

Fig. 3 FEA results: **a** stress distribution; **b** strain distribution

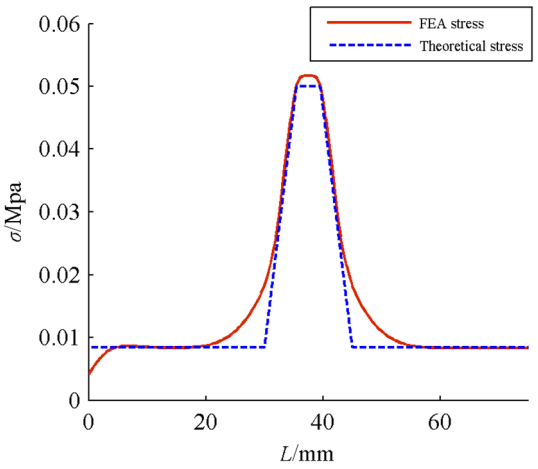

Fig. 4 Axial stress distribution

$C_{\alpha\text{-}Mz}$, shear compliance $C_{y\text{-}Fy}$ and axial compliance $C_{x\text{-}Fx}$, as illustrated in Fig. 6a. And the axial compliance proportions are much larger than other's. As depicted in Fig. 6b, axial compliance calculation errors are relative large. While shear and bending compliance calculation errors increase first and then decrease sharply. In addition, when the value of t/L is more than 0.9, these two compliance calculation errors increase again.

The compliance proportion is multiplied by the compliance calculation error as an evaluation factor. Figure 7a shows the evaluation factors of the second parts. It shows that the axial evaluation factors exhibit an increase from 1.5 to about 6.5. These values are relative large, and stress concentration should be considered when calculating axial compliance. While the shear and bending evaluation factors are almost zero, and thus the stress concentration can be ignored when calculating these compliances. In contrast, the evaluation factors of the third parts are depicted in Fig. 7b. It can be seen that the evaluation factors are all below 1, especially the evaluation factors of the bending compliance, which are almost zero. It indicates that the influence on these parts is small, and the stress concentration can be ignored. The reason is that the third parts are away from the hinge, and the cross-section is constant. Meanwhile, similar results can be derived when R/L changed due to the proposed reason, but not illustrated herein.

3.2 Empirical compliance equations

According to the analysis above, we can see that the stress concentration should be considered when deriving the axial compliance equation, while it can be ignored when calculating the other compliance components. Subsequently, the compliance components of corner-filleted flexure hinges are then obtained by using FEA, the derivation of these equations can be shown as follows.

3.2.1 Axial compliance

Based on the previous analysis, to calculate the axial compliance, both corner-filleted hinge and the rigid beams are

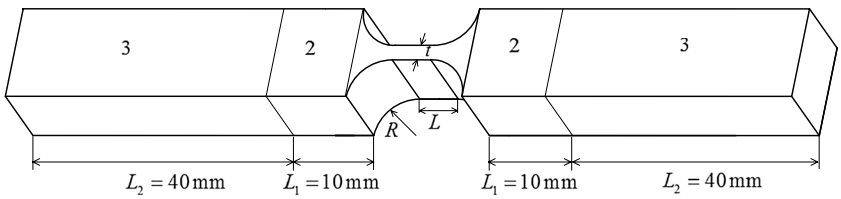

Fig. 5 Corner-filleted flexure hinge with particular rigid beams

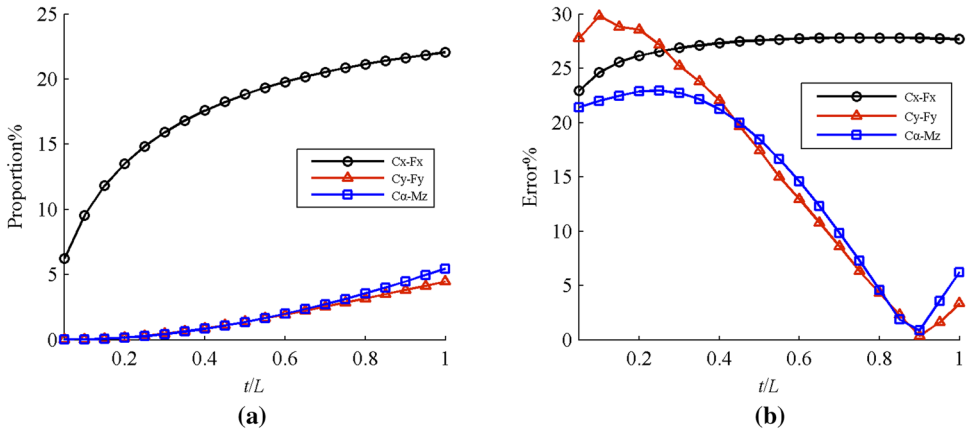

Fig. 6 Results of the second parts: **a** compliance proportions; **b** compliance calculation errors

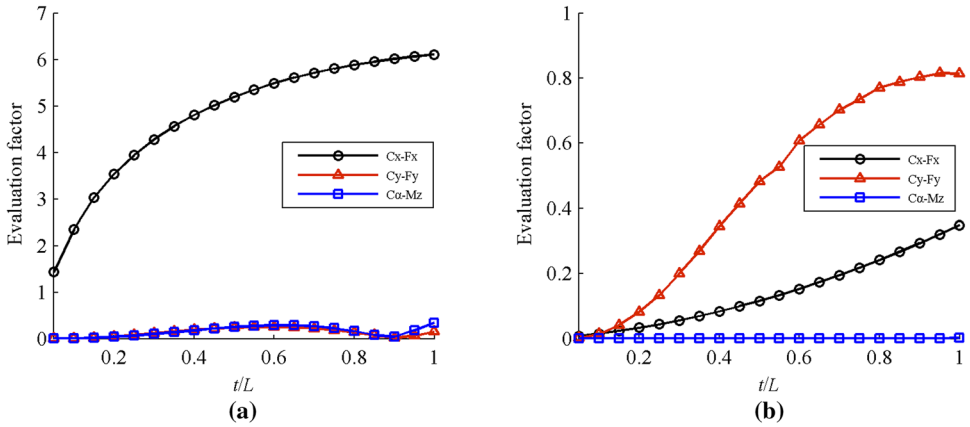

Fig. 7 Trends of evaluation factors: **a** the second parts; **b** the third parts

all considered. The restraint, geometrical parameters and external load of a selected corner-filleted hinge are shown in Fig. 8. External load is applied on surface D, and surface A is fixed.

Figure 4 shows axial stress distribution along the *x*-axis. We can see that it is comprised of two regions. One is a variable region (above the straight line) related to the corner-filleted hinge. The other one is a constant region (below the straight line) which is almost in accordance with the basic theoretical stress curve. The uniform distributed load is applied on the surface D of the hinge for keeping the deformation of the rigid beams constant, and thus the deformation of the constant region can be derived easily. Meanwhile, according to the theories of mechanisms of materials, the equation involved all the geometrical parameters affecting the deformation of the variable region can also be obtained. Without loss of generality, α represents the total deformation of the selected hinge, α_s denotes the deformation of the constant region (the rigid beams), and α_x denotes the deformation of the variable region (the corner-filleted hinge). Then, the proposed deformations can be expressed as, respectively

$$\alpha = \alpha_s + \alpha_x \tag{5}$$

$$\alpha_s = \frac{FL_t}{ES} = \frac{F(2R + L + 2W)}{ED(2R + t)} = \frac{PL_t}{E} \tag{6}$$

$$\alpha_x = k\frac{PL^m R^i}{Et^j} \tag{7}$$

where L_t denotes the total length, F is the axial load, S is the area, E is the Young's modulus, and k denotes the constant coefficient which is independent of geometrical parameters, material properties and the loads; m, i and j are the indexes corresponding to the geometrical parameters.

The external load σ is 1 Mpa, as illustrated in Fig. 8. Deformation generated along axial direction can be obtained by FEA. In addition, geometrical parameters are taken as $W = 30$ mm, $D = 10$ mm. Firstly, the hinge length is 5 mm, the hinge radius is 5 mm, and the value of t is varied from 0.5 mm to 5 mm to analyze the relationship between t and α_x, as shown in Fig. 9. It indicates that they have the exponential relationship. The logarithm of the values of the horizontal and vertical coordinate are obtained. And then least square method is applied. To obtain the unified dimension, the index is revised, and $j = 0.6890$. Then, the hinge length is 5 mm,the hinge thickness is 1 mm, and the value of R is varied from 1 mm to 10 mm to analyze the relationship between R and α_x. Finally, the hinge radius is 5 mm, the hinge thickness is 1 mm, and the value of L is varied from 0.5 to 5 mm to analyze the relationship between L and α_x. Similarly, the index i and m can be obtained as 1.3129 and 0.3761, respectively.

To get the proposed k, $f(k)$ could be expressed as

$$f(k) = \left(\sum_i \alpha_{xi} - k\frac{PL^m R^i}{Et_i^j}\right)^2 \tag{8}$$

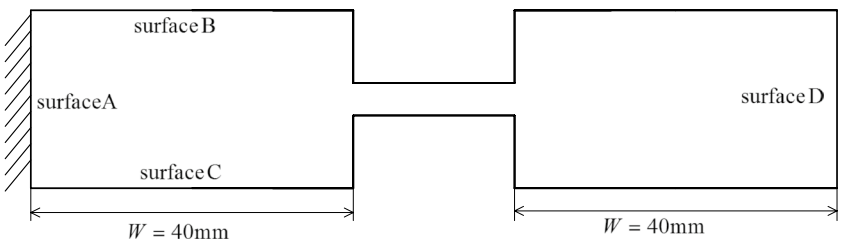

Fig. 8 Restraint, geometrical parameters and external load

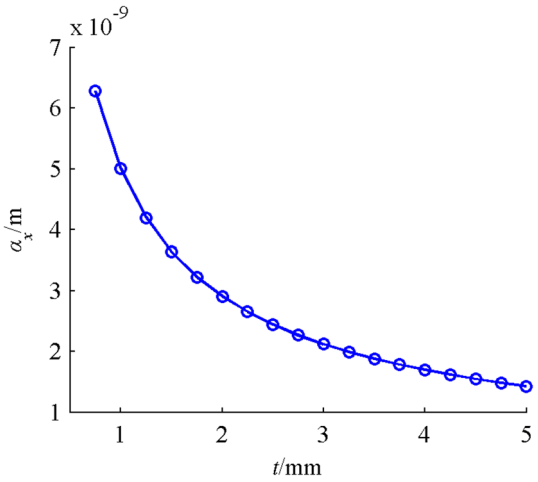

Fig. 9 Relationship between α_x and t

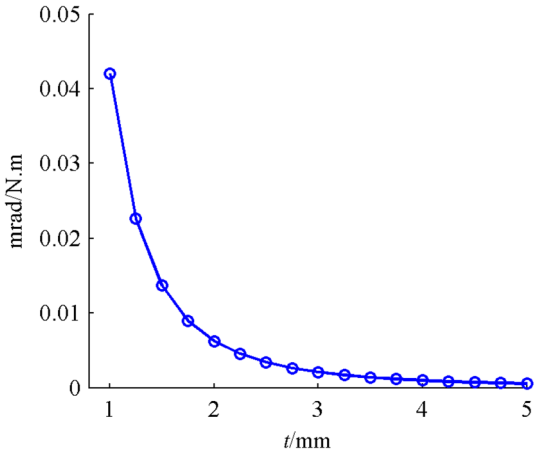

Fig. 10 Relationship between θ and t

For minimizing $f(k)$, k could be given as

$$k = \frac{\sum_i \left(\frac{pL^m R^i}{Et_i^j}\alpha_{xi}\right)}{\sum_i \left(\frac{PL^m R^i}{Et_i^j}\right)^2}. \tag{9}$$

The constant coefficient can be obtained as $k_t = 6.6585$, $k_R = 7.0307$ and $k_L = 6.9544$ in terms of the relationship $\alpha_x - t$, $\alpha_x R$ and $\alpha_x L$, and then the average value can be calculated as $k = 6.8812$. Hence, the total axial deformation and the axial compliance can be given as follows

$$\alpha = \frac{F}{ED(2R+t)}\left[6.8812 \cdot R \cdot \left(\frac{R}{t}\right)^{0.3129} \cdot \left(\frac{L}{t}\right)^{0.3761} + L + 2W + 2R\right] \tag{10}$$

$$C_{x-Fx} = \frac{1}{ED(2R+t)}\left[6.8812 \cdot R \cdot \left(\frac{R}{t}\right)^{0.3129} \cdot \left(\frac{L}{t}\right)^{0.3761} + L + 2W + 2R\right]. \tag{11}$$

where k is the constant coefficient which is independent of the geometrical parameters, material properties and the loads; m, i and j are the indexes corresponding to the geometrical parameters.

Similarly, the deformation along the x-axis can be read by FEA directly. Geometrical parameters are selected as $W = 30$ mm, $D = 10$ mm. Firstly, the hinge length is 5 mm, the hinge radius is 5 mm, and the value of t is varied from 1 mm to 5 mm to analyze the relationship between t and θ, as shown in Fig. 10. To obtain the unified dimension, the index is revised, and $j = 2.6676$. The index m and i can be obtained as 0.4833 and 0.1843, respectively. According to the principle of minimizing variance, coupled with the relationships $\theta - t$, $\theta - R$ and $\theta - L$, the constant coefficients k_t, k_R and k_L are derived. And then the average value can be calculated as $k = 29.7502$.

3.2.2 Bending compliance

According to the previous analysis, stress concentration can be ignored when calculating bending compliance. Therefore, only the corner-filleted flexure hinge between the two rigid beams is selected. As shown in Fig. 8, a bending moment is impacted on the surface D, and the other three surfaces could be fixed. According to the theories of mechanisms of materials, the equation involved all the geometrical parameters affecting θ can be written as

$$\theta = k \cdot \frac{M}{ED} \cdot \frac{L^m R^i}{t^j} = K \cdot \frac{P}{E} \cdot \frac{L^m R^i}{t^j} \tag{12}$$

Therefore, the compliance equations of $C_{\alpha-Mz}$ can be expressed as

$$C_{\alpha-Mz} = \frac{29.7502}{EDt^2} \cdot \left(\frac{L}{t}\right)^{0.4833} \cdot \left(\frac{R}{t}\right)^{0.1843}. \tag{13}$$

Similarly, the indexes corresponding to the geometrical parameters can be obtained by using exponential models and least square method. The indexes corresponding to the geometrical parameters t, L, and R can be obtained as 2.6720, 0.7693 and 0.9027, respectively. While the constant coefficient can be obtained by the principle of minimizing variance, and it is 43.9226. The compliance equation of $C_{y\text{-}Mz}$ can be expressed as

$$C_{y-Mz} = \frac{43.9226}{EDt} \cdot \left(\frac{L}{t}\right)^{0.7693} \cdot \left(\frac{R}{t}\right)^{0.9027}. \quad (14)$$

3.2.3 Shear compliance

According to the previous analysis, stress concentration can be ignored when calculating shear compliance. Therefore, only the corner-filleted flexure hinge between the two rigid beams is considered. Similarly, for the compliance $C_{y\text{-}Fy}$, the indexes corresponding to the geometrical parameters t, L, and R can be obtained as 2.6547, 1.0770 and 1.5777, respectively. The constant coefficient is 75.3279. In addition, for the compliance $C_{\alpha\text{-}Fy}$, the indexes corresponding to the geometrical parameters t, L, and R can be obtained as 2.6757, 0.7712 and 0.9044, respectively. The constant coefficient is 43.6875. Thus, $C_{y\text{-}Fy}$ and $C_{\alpha\text{-}Fy}$ can be expressed as, respectively

$$C_{y-Fy} = \frac{75.3279}{ED} \cdot \left(\frac{L}{t}\right)^{1.0770} \left(\frac{R}{t}\right)^{1.5777} + \frac{\alpha \cdot E}{G} \cdot C_{x-Fx} \quad (15)$$

$$C_{\alpha-Fy} = \frac{43.6875}{EDt} \cdot \left(\frac{L}{t}\right)^{0.7712} \cdot \left(\frac{R}{t}\right)^{0.9044}. \quad (16)$$

3.3 Validation

In order to verify the accuracy and validity of the empirical compliance equations derived above initially, the errors between the results calculated by empirical equations and FEA are analyzed. Without loss of generality, corner-filleted flexure hinges are selected. $R = 10$ m, $L = 5$ mm, $W = 30$ m, $D = 10$ mm, and the value of t is varied from 0.5 to 10 mm. Errors between the results derived from the empirical equations of main compliance components and FEA are illustrated in Fig. 11. The calculation errors of the three main compliance components are all below 10%, and it proves that the values calculated by empirical equations are almost coincident with the FEA values.

4 Circular and rectangular flexure hinges

Geometrical parameters of the rectangular flexure hinge are shown in Fig. 12, including the hinge length L, the hinge thickness t, the side height h, the width W, the total height H and the total depth D [23].

According to the method of deriving compliance equations for the corner-filleted flexure hinge, empirical compliance equations for the rectangular flexure hinge can be expressed as [23]

$$C_{x-Fx} = \frac{1}{ED(2h+t)}\left[4 \cdot h \cdot \left(\frac{h}{t}\right)^{0.0709} \cdot \left(\frac{L}{t}\right)^{0.7515} + L + 2W\right], \quad (17)$$

$$C_{\alpha-Mz} = \frac{16.5350}{EDt^2} \cdot \left(\frac{L}{t}\right)^{0.8856}, \quad (18)$$

$$C_{y-Fy} = \frac{5.2749}{ED} \cdot \left(\frac{h}{t}\right)^{0.0124} \cdot \left(\frac{L}{t}\right)^{2.8996} + \frac{\alpha \cdot E}{G} \cdot C_{x-Fx}, \quad (19)$$

$$C_{y-Mz} = C_{\alpha-Fy} = \frac{8.3802}{EDt} \cdot \left(\frac{L}{t}\right)^{1.8826}, \quad (20)$$

Geometrical parameters of the circular flexure hinge are shown in Fig. 13, including the hinge thickness t, the hinge radius R, the width W, the total height H and the total depth D [6].

Empirical compliance equations for circular flexure hinges in terms of stress concentration can be written as [6]

$$C_{x-Fx} = \frac{1}{ED(2R+t)}\left[3.908R\left(\frac{R}{t}\right)^{0.622} + 2(R+W)\right] \quad (21)$$

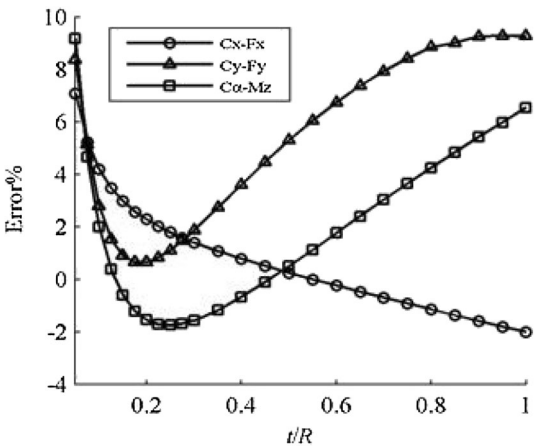

Fig. 11 Errors generated from empirical equations

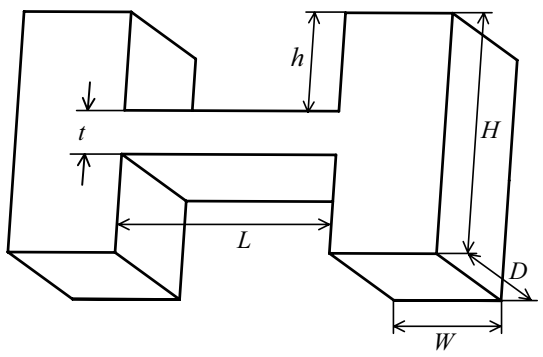

Fig. 12 Geometrical parameters of the rectangular flexure hinge

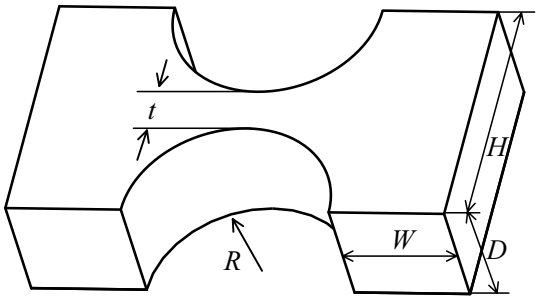

Fig. 13 Geometrical parameters of the circular flexure hinge

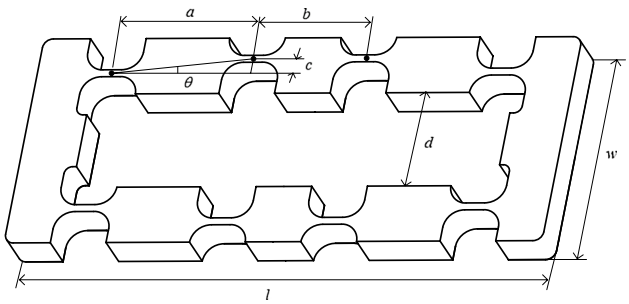

Fig. 14 Structure of the developed mechanism

$$C_{\alpha-Mz} = \frac{16}{EDt^2}\left(\frac{R}{t}\right)^{0.43} \tag{22}$$

$$C_{\alpha-Fy} = \frac{16.58}{EDt}\left(\frac{R}{t}\right)^{1.427} \tag{23}$$

$$C_{y-Fy} = \frac{17.3}{ED}\left(\frac{R}{t}\right)^{2.412} + \frac{\mu E}{G}C_{x-Fx} \tag{24}$$

$$C_{\alpha-Fy} = \frac{16.55}{EDt}\left(\frac{R}{t}\right)^{1.429}. \tag{25}$$

5 Conventional single-axis flexure hinges

The rectangular, circular, and corner-filled flexure hinges are especially conventional, and thus they have been widely used in applications. According to Sects. 3 and 4, we can see that the empirical compliance equations for conventional single-axis flexure hinges have similar forms, and therefore these equations can be unified. The axial compliance of conventional single-axis flexure hinges can be given as

$$C_{x-Fx} = \frac{c_x t}{EDH}\left(f_x(r,R,t) + L_z\right) \tag{26}$$

where c_x is the constant coefficient, H is the total height of rigid beams, L_z is the total length of flexure hinge, and $f_x(r,R,t)$ is the exponential model related to corresponding geometrical parameters.

The shear compliance of conventional single-axis flexure hinges can be given as

$$C_{y-Fy} = \frac{c_y}{ED}f_y(r,R,t) + \frac{\alpha E}{G}C_{x-Fx} \tag{27}$$

where c_y is the constant coefficient, and $f_y(r,R,t)$ is the exponential model related to corresponding geometrical parameters.

The bending compliance of conventional single-axis flexure hinges can be given as

$$C_{\alpha-Mz} = \frac{c_z}{EDt^2}f_z(r,R,t) \tag{28}$$

where c_z is the constant coefficient, and $f_z(r,R,t)$ is the exponential model related to corresponding geometrical parameters.

Similarly, the compliance equations of $C_{y\text{-}Mz}$ and $C_{\alpha\text{-}Fy}$ can be expressed as

$$C_{y-Mz} = C_{\alpha-Fy} = \frac{c_{yz}}{EDt}f_{yz}(r,R,t) \tag{29}$$

where c_{yz} is the constant coefficient, and $f_{yz}(r,R,t)$ is the exponential model related to corresponding geometrical parameters.

6 Applications

Corner-filleted flexure hinge are typical single-axis hinges, and thus they are chosen as basic elements of bridge-type flexure-based mechanisms. These mechanisms can be used to constitute the piezo-driven stages to magnify the displacement of piezo actuators. The displacement of a piezo actuator is limited to several tens of microns, and thus applications with several tens to several hundreds of microns require these bridge-type flexure-based mechanisms. Specifically, corner-filleted hinges with two rigid beams can be considered as a whole part which can be used to form the mechanism. As shown in Fig. 14, the developed mechanism is comprised of eight corner-filleted hinges and several rigid beams. Its compliance and displacement amplification ratios are further investigated to verify the previous analysis.

Table 1 lists the key geometrical parameters and material properties. The eight corner-filleted hinges with rigid beams possess same characteristics such as material, structure, and geometrical parameters.

Table 1 Characteristics of the developed mechanism

Characteristics	
Young's modulus, E (GPa)	210
Poisson's ratio, v	0.30
a (mm)	30
b (mm)	37.5
d (mm)	30
l(mm)	145
L (mm)	5
t (mm)	2
R (mm)	5
W (mm)	5
D (mm)	10

As the boundary conditions of the developed mechanism can be easily determined, coupled with the characteristics of flexure-based mechanisms, the results obtained by FEA must be accurate. FEA is carried on by the software ANSYS 14.0. As shown in Fig. 15, there are four main surfaces, two input points and a displacement output point. The displacement output point is on the surface D, while the two input points are on the surface A and C, respectively. External forces can be applied on the two input points.

The characteristics of the developed flexure-based mechanism depend on angle θ when the length of the mechanism is fixed. The comparison between the theoretical value derived from the empirical compliance equations and the FEA value is studied, and the results are shown in Fig. 16. As shown in Fig. 16a, an exponential relationship exists between the input compliance and the angle θ. As illustrated in Fig. 16b, the output compliance of the mechanism will increase when the value of θ increases, and they maintain a linear relationship. Generally, the theoretical results are in accord with FEA results, and it proves that the empirical compliance equations are accurate.

The amplification ratios of the developed flexure-based mechanism are determined by FEA and the empirical compliance equations. The theoretical arithmetic contains the values in terms of the rigid beams and that without rigid beams. And the results obtained by the two methods are illustrated in Fig. 17. There are

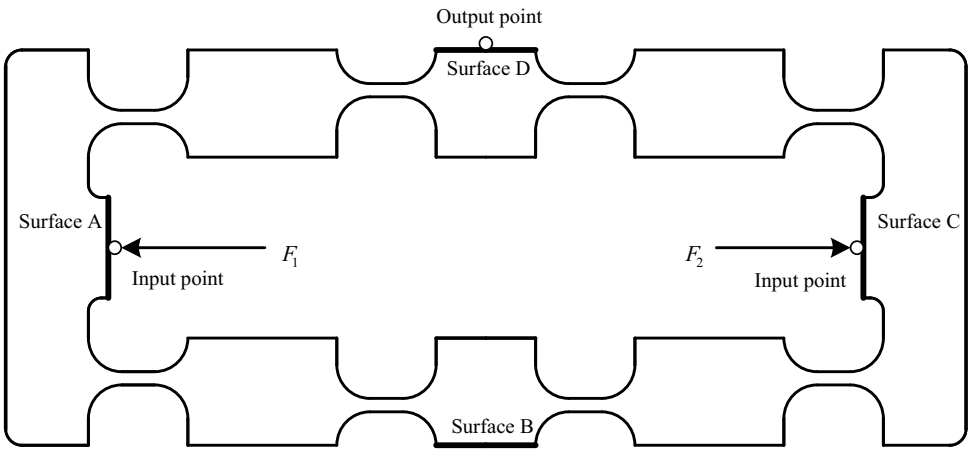

Fig. 15 Detail of the developed mechanism

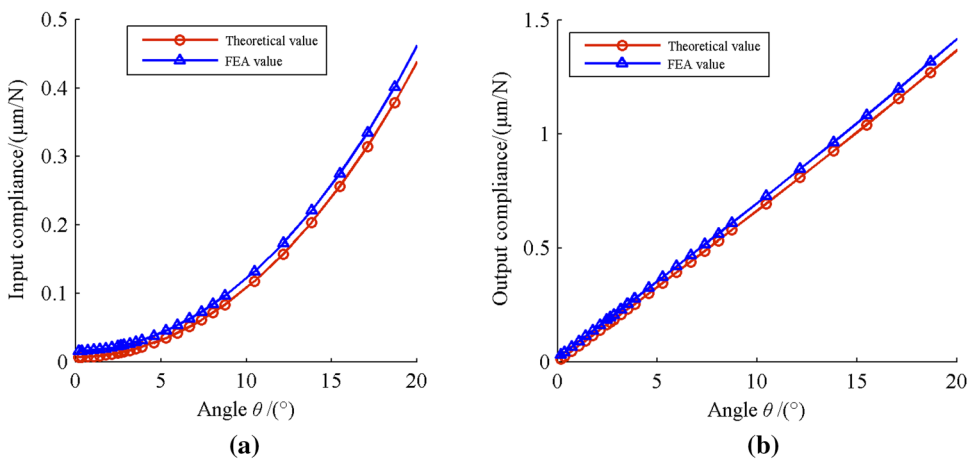

Fig. 16 Compliance of the amplify mechanism: **a** input compliance; **b** output compliance

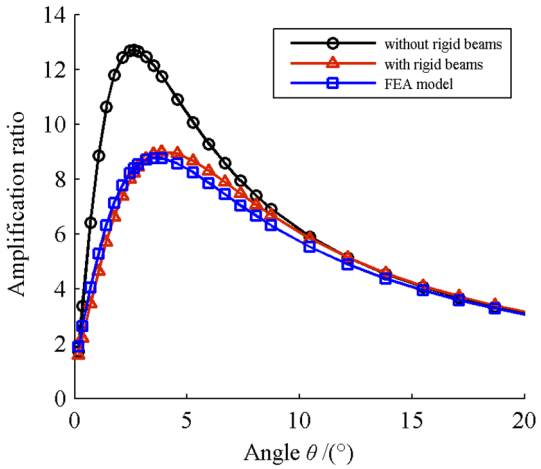

Fig. 17 Displacement amplification ratios

three wave lines. For the black line, it indicates that the amplification ratios determined by ignoring the rigid beams increase when the value of θ is less than 2.5, and then they decrease when the value of θ is more than 2.5. For the blue and red lines, they almost coincide, and they increase first and then decrease. In addition, when the value of θ is less than 3, the theoretical ratios determined in terms of the rigid beams is smaller than the ratios determined by FEA. By contrast, when the value of θ is over 3, the theoretical ratios are larger. What's more, the theoretical ratios determined in terms of the rigid beams are in accordance with the ratios determined by FEA, while the theoretical ratios determined without the rigid beams are much larger than their ratios. It demonstrates that the rigid beams should be considered when calculating the amplification ratios of this developed flexure-based mechanism, and the proposed compliance method and the corresponding equations are accurate.

7 Conclusions

According to the analysis of stress concentration, the relationship between the deformation and geometrical parameters can be obtained, and thus the exponential model is proposed. Based upon, the empirical compliance equations for three hinges and the conventional hinges are determined. A bridge-type flexure-based mechanism is then designed by using eight hinges with rigid beams. Its characteristics are then determined by FEA and these equations. From what we have discussed above, we can easily arrive at the following conclusions:

1. For single-axis flexure hinges, stress concentration is in relation to the axial compliance but not in relation to the bending compliance and shear compliance.
2. For single-axis flexure hinges, empirical compliance equations determined by exponential model can be unified.
3. The amplification ratios calculated by FEA are in accordance with the theoretical arithmetic derived from empirical equations. It indicates that the compliance calculation method and the corresponding equations are valid.

Acknowledgements This work was supported by Beijing Natural Science Foundation (3194044), and Beijing Postdoctoral Research Foundation of China (2017-ZZ-034).

Compliance with ethical standards

Conflict of interest The authors declare that they have no conflict of interest.

References

1. Lobontiu N (2010) Compliant mechanisms:design of flexure hinges. CRC Press, Boca Raton, pp 2–15
2. Wan S, Zhang Y, Xu Q (2017) Design and development of a new large-stroke XY compliant micropositioning stage. Proc IMechE Part C J Mech Eng Sci 231:3263–3276
3. Liu M, Zhang X, Fatikow S (2017) Design and analysis of a multi-notched flexure hinge for compliant mechanisms. Precis Eng 48:292–304
4. Clark L, Shirinzadeh B, Pinskier J et al (2018) Topology optimization of bridge input structures with maximal amplification for design of flexure mechanisms. Mech Mach Theory 122:113–131
5. Hopkins JB, Vericella JJ, Harvey CD (2014) Modeling and generating parallel flexure elements. Precis Eng 38:525–537
6. Li TM, Zhang JL, Jiang Y (2015) Derivation of empirical compliance equations for circular flexure hinge considering the effect of stress concentration. Int J Precis Eng Manuf 16:1735–1743
7. Elgammal AT, Fanni M, Mohamed AM (2017) Design and analysis of a novel 3d decoupled manipulator based on compliant pantograph for micromanipulation. J Intell Robot Syst 87:43–57
8. Pinskier J, Shirinzadeh B, Clark L et al (2016) Design, development and analysis of a haptic-enabled modular flexure-based manipulator. Mechatronics 40:156–166
9. Verma S, Kim WJ, Shakir H (2015) Multi-axis maglev nanopositioner for precision manufacturing and manipulation applications. IEEE Trans Ind Appl 41:1159–1167
10. Hao GB, Li H, Kavanagh R (2016) Design of decoupled, compact, and monolithic spatial translational compliant parallel manipulators based on the position space. Proc IMechE Part C J Mech Eng Sci 230:367–378
11. Choi KB, Lee JJ, Kim GH et al (2018) Amplification ratio analysis of a bridge-type mechanical amplification mechanism based on a fully compliant model. Mech Mach Theory 121:355–372
12. Clark L, Shirinzadeh B, Zhong Y et al (2016) Design and analysis of a compact flexure-based precision pure rotation stage without actuator redundancy. Mech Mach Theory 105:129–144

13. Huang H, Fu L, Zhao H et al (2013) Note: a novel rotary actuator driven by only one piezoelectric actuator. Rev Sci Instrum 84:096105
14. Yong YK, Lu TF (2009) Comparison of circular flexure hinge design equations and the derivation of empirical stiffness formulations. In: IEEE/ASME international conference on advanced intelligent mechatronics, IEEE, Singapore, 14–17 July 2009, pp 510–515
15. Schotborgh WO, Kokkeler FGM, Tragter H et al (2005) Dimensionless design graphs for flexure elements and a comparison between three flexure elements. Precis Eng 29:41–47
16. Acer M, Sabanovic A (2011) Comparison of circular flexure hinge compliance modeling methods. In: IEEE international conference on mechatronics, IEEE, Istanbul, Turkey, 13–15 Apr 2011, pp 271–276
17. Paros JM (1965) How to design flexure hinges. Mach Des 37:151–156
18. Smith ST, Badami VG, Dale JS et al (1997) Elliptical flexure hinges. Rev Sci Instrum 68:1474–1483
19. Tian Y, Shirinzadeh B, Zhang D et al (2010) Three flexure hinges for compliant mechanism designs based on dimensionless graph analysis. Precis Eng 34:92–100
20. Lobontiu N, Garcia E, Hardau M et al (2004) Stiffness characterization of corner-filleted flexure hinges. Rev Sci Instrum 75:4896–4905
21. Meng Q, Li Y, Xu J (2013) New empirical stiffness equations for corner-filleted flexure hinges. Mech Sci 4:345–356
22. Yong YK, Lu TF, Handley DC (2008) Review of circular flexure hinge design equations and derivation of empirical formulations. Precis Eng 32:63–70
23. Li TM, Du YS, Jiang Y, et al (2016) Empirical compliance equations for constant rectangular cross section flexure hinges and their applications. In: Mathematical problems in engineering